

L. M. Rickett · M. G. Blyth

# Flow in a slowly tapering channel with oscillating walls

Received: 30 April 2014 / Revised: 5 August 2014  
© Springer-Verlag Wien 2014

**Abstract** The flow of a fluid in a channel with walls inclined at an angle to each other is investigated at arbitrary Reynolds number. The flow is driven by an oscillatory motion of the wall incorporating a time-periodic displacement perpendicular to the channel centreline. The gap between the walls varies linearly with distance along the channel and is a prescribed periodic function of time. An approximate solution is constructed assuming that the angle of inclination of the walls is small. At leading order, the flow corresponds to that in a channel with parallel, vertically oscillating walls examined by Hall and Papageorgiou (J. Fluid Mech. 393:59–87, 1999). A careful study of the governing partial differential system for the first-order approximation controlling the tapering flow due to the wall inclination is conducted. It is found that as the Reynolds number is increased from zero the tapering flow loses symmetry and undergoes exponential growth in time. The loss of symmetry occurs at a lower Reynolds number than the symmetry breaking for the parallel-wall flow. A window of asymmetric, time-periodic solutions is found at higher Reynolds number, and these are reached via a quasiperiodic transient from a given set of initial conditions. Beyond this window, stability is again lost to exponentially growing solutions as the Reynolds number is increased.

## 1 Introduction

Idealised theoretical studies of flow in channels and pipes have established a powerful working base from which to make valuable predictions about more complex flows in more practically applicable flow scenarios. In particular, flow in pulsating pipes and channels has been used to model blood flow in coronary arteries [12] and transmural revascularisation in heart tissue [15, 16], whilst oscillating flow in a tapered channel has been used to model ventilation in the lung [4]. The present investigation, which considers flow in a slightly tapering channel with oscillating walls, was motivated at an early stage by the desire to model the motion of digestive juices in the upper part of the stomach, whose diameter tends to decrease as the lower part of the stomach is approached. In the upper part of the stomach, digestive fluid and any suspended food bolus are subjected to slight and gentle pulsations of the stomach walls [9]. In this flow, the Reynolds number is rather small and the corresponding model flow in the tapering channel can be described very simply to a first approximation. Flow at higher Reynolds number lies outside the regime of interest for digestive flow in the upper stomach, but it has an interesting mathematical structure and forms the core of the current study.

---

L. M. Rickett · M. G. Blyth (✉)  
School of Mathematics, University of East Anglia, Norwich, UK  
E-mail: m.blyth@uea.ac.uk

*Present Address:*  
L. M. Rickett  
The Sainsbury Laboratory, Norwich, UK  
E-mail: Lydia.Rickett@sainsbury-laboratory.ac.uk

Hall [5] considered unsteady flow in a pipe of slowly varying cross-section due to an oscillatory pressure difference applied between the ends. Of particular relevance to the present work is the study by Hall and Papageorgiou [6], henceforth referred to as HP, of flow in an infinite channel with parallel walls where the gap between the walls is a prescribed periodic function of time, so that the walls are moving vertically up and down. For this problem, a solution can be sought in which the axial velocity is decomposed into a form with the coordinate along the channel axis,  $x$  say, multiplied by a nonlinear function of both time and the vertical coordinate across the channel. A Reynolds number defined on the wall frequency, the average gap between the walls, and the kinematic viscosity of the fluid, and the wall oscillation amplitude as a fraction of the average channel width constitutes the two-dimensional parameters in the problem. At sufficiently small Reynolds number the flow is unique, it is symmetric about the channel centreline, and it is synchronous with the wall motion. When the Reynolds number is increased, a sequence of bifurcations leads to an increasingly complex solution space. First, a symmetry-breaking bifurcation introduces a stable asymmetric flow solution which is synchronous with the wall motion. At higher Reynolds number, this asymmetric flow loses stability and becomes quasiperiodic after a Hopf bifurcation introduces a new frequency which is incommensurate with that of the wall motion. Subsequent bifurcations lead to chaotic flow solutions. In later work, Blyth et al. [1] considered the similar problem of flow in a pipe whose radius is a periodic function of time. Again a solution with a stagnation-type structure can be sought and intricate flow dynamics appear as the Reynolds number is increased from zero.

For the channel problem studied by HP, Secomb [12] showed that a second flow can be superimposed on the primary flow (with axial velocity proportional to  $x$ ) without changing the primary flow in any way. The secondary flow, which may include an arbitrary pressure gradient, satisfies an equation with coefficients determined by the solution to the primary flow, as so is subservient to it in this way. In a recent study, Espin and Papageorgiou [2], hereinafter referred to as EP, investigated solutions to this secondary flow system. They found that the secondary flow (for constant pressure gradient) experiences a symmetry-breaking bifurcation at a lower Reynolds number than the primary flow. At slightly higher Reynolds number, the flow destabilises and experiences unbounded exponential growth in time.

In the present paper, we investigate the HP problem when the channel walls are tilted at an angle to the horizontal so that the gap between the walls tapers linearly with  $x$  along the channel. By assuming that the angle of inclination of the walls is small, of order  $\delta$  say, we are able to expand in  $\delta$  to obtain a pair of partial differential systems governing the adjustment to the HP flow due to the taper. Similar to the system studied by EP, the equations depend via their coefficients on the HP flow and so are expected to exhibit complex dynamical behaviour as the Reynolds number increases. Using a numerical method, we conduct a wide-ranging study across parameter space to determine the flow dynamics of the tapering flow adjustment.

## 2 Problem formulation

We consider the flow of an incompressible fluid of viscosity  $\mu$  and density  $\rho$  in a channel whose width is a periodic function of time and varies slowly and linearly with distance along the channel centreline. Referring to the axes shown in Fig. 1, the channel walls are located at  $y = \pm H(x, t)$ , with

$$H = H_0(t) + \delta x H_1(t), \quad (1)$$

where  $\delta$  is a small parameter and the forms of  $H_0$  and  $H_1$  will be given below. Here and elsewhere, variables have been made dimensionless using  $a$ , the typical channel width, as the reference length scale,  $1/\omega$ , where  $\omega$  is the frequency of the wall motion, as the timescale, and  $\mu\omega$  as the pressure scale. The Reynolds number for the flow is defined to be

$$R = \frac{a^2\omega}{\nu}, \quad (2)$$

where  $\nu = \mu/\rho$  is the kinematic viscosity of the fluid. To describe the flow, it will be convenient to define a streamfunction  $\Psi(x, y, t)$  in the usual way so that  $u = \Psi_y$  and  $v = -\Psi_x$ , where  $u$  and  $v$  are the horizontal and vertical components of velocity, respectively.

In the simplest case,  $\delta = 0$ , the channel walls are parallel and the problem reduces to that introduced by Secomb [12] and studied extensively by HP on the assumption that

$$H_0(t) = 1 + \Delta \cos 2t, \quad (3)$$

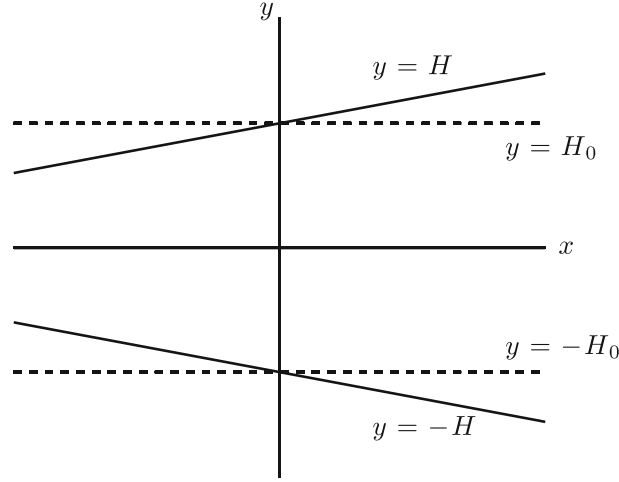


**Fig. 1** Schematic of the channel geometry. The inclined walls are located at  $y = \pm H(x, t)$ . The *broken lines* indicate the parallel-wall HP flow positions at  $y = \pm H_0(x, t)$

for constant  $0 < \Delta < 1$ . Subsequently, EP examined the effect of an imposed streamwise pressure gradient driving an additional flow component which is in part controlled by, but which does not affect, the HP flow. Written together, the combined HP and EP flow structure is expressed in the form proposed by Secomb [12],

$$\Psi(x, y, t) = \Psi_0 = xF_0(y, t) + \int^y G_0(\xi, t) d\xi, \quad (4)$$

and

$$p(x, y, t) = p_0 = \frac{1}{2}x^2\alpha_0(t) + x\beta_0(t) + \gamma_0(y, t), \quad (5)$$

where  $p$  is the fluid pressure. Substituting into the  $x$ -component of the Navier–Stokes equation, and differentiating once with respect to  $y$ , the governing equation for the HP streamfunction  $F_0$  is obtained as

$$F_{0yyt} + F_{0y}F_{0yy} - F_0F_{0yyy} = \frac{1}{R}F_{0yyyy}. \quad (6)$$

The boundary conditions are

$$F_{0y} = 0, \quad F_0 = \mp \dot{H}_0 \quad (7)$$

at  $y = \pm H_0(t)$ . Once a solution to the system (6), (7) has been identified, the pressure components  $\alpha_0$  and  $\gamma_0$  can be found readily from the  $x$ - and  $y$ -components of the Navier–Stokes equation. The pressure gradient imposed by EP, namely  $\beta_0(t)$ , drives a parasitic flow represented by the streamfunction component  $G_0$ , which satisfies the equation,

$$G_{0t} + F_{0y}G_0 - F_0G_{0y} = -\frac{1}{R}\beta_0 + \frac{1}{R}G_{0yy}, \quad (8)$$

and is subject to the boundary conditions

$$G_0 = 0 \quad (9)$$

at  $y = \pm H_0$ . This is the system studied in depth by EP. Note that  $G_0$  is determined by the solution to (8), (9) within an arbitrary but dynamically irrelevant function of time.

When  $\delta$  is small and the channel walls are slightly tilted, we seek a solution for the streamfunction and pressure in the form

$$\Psi = \Psi_0(x, y, t) + \delta \psi_1(x, y, t) + \dots, \quad p = p_0(x, y, t) + \delta p_1(x, y, t) + \dots, \quad (10)$$

where

$$\Psi_1 = x^2 F_1(y, t) + \int^y G_1(\xi, t) d\xi, \quad p_1 = \frac{1}{3}x^3 \alpha_1(t) + x\beta_1(y, t) + \gamma_1(t). \quad (11)$$

These expansions are valid over a restricted range in  $x$ ; further comment on this point will be made in Sect. 6. Substituting into the  $x$ -component of the Navier–Stokes equation, differentiating with respect to  $y$ , and retaining terms at  $O(\delta)$ , we obtain the governing equation for  $F_1$ ,

$$F_{1yyt} - 2F_{0yyy}F_1 + F_{0yy}F_{1y} + 2F_{0y}F_{1yy} - F_0F_{1yyy} = \frac{1}{R}F_{1yyy}. \quad (12)$$

The boundary conditions are

$$F_1 = \mp \frac{1}{2}\dot{H}_1, \quad F_{1y} = \mp F_{0yy}H_1 \quad (13)$$

at  $y = \pm H_0$ . Similarly, we derive the system for  $G_1$ ,

$$G_{1t} + F_{0y}G_1 - F_0G_{1y} = \frac{1}{R}(-\beta_1 + 2F_{1y}) + \frac{1}{R}G_{1yy} \quad (14)$$

with boundary conditions

$$G_1 = -\dot{H}_0H_1 \quad (15)$$

at  $y = \pm H_0$ . We note that if  $H_1$  is taken to be constant the simple rescaling  $F_1 \rightarrow H_1 F_1$  removes  $H_1$  from the problem in (12)–(15) and its particular value needs not to be considered further (note that in subsequent calculations presented in this paper,  $H_1$  will be taken as constant and so this scaling applies). Note that (14) is similar in form to the parasitic equation (8) studied by EP, but the boundary conditions at the walls are different, and in (14) the pressure gradient term  $\beta_1$  is not free to choose but depends on the solutions to (6) and (12); in fact, it is obtained by integrating the relation  $\beta_{1y} = R(2F_{1t} - 2F_0F_{1y}) - 2F_{1yy}$ , which comes from the  $y$ -component of the Navier–Stokes equation.

For small Reynolds number, the HP solution to (6), (7) is given by

$$F_0 = \frac{1}{2}\dot{H}_0 \eta (\eta^2 - 3) + O(R), \quad (16)$$

where  $\eta = y/H_0$ . As noted by HP, the form (16) means that at any fixed  $x$  and fixed  $t$ , the horizontal velocity profile across the channel coincides with that for Poiseuille flow. For small  $R$ , the tapering flow solution is given by

$$F_1 = \frac{1}{4}\dot{H}_1 \eta (\eta^2 - 3) - \frac{3}{2} \frac{\dot{H}_0 H_1}{H_0} \eta (\eta^2 - 1) + O(R). \quad (17)$$

Similar to (16), the first term in (17) corresponds locally to a Poiseuille flow profile in the horizontal direction.

In this paper, our interest mainly lies in studying the dynamics of the primary first-order flow system (12), (13) at arbitrary Reynolds number. These are examined by numerical integration using a method to be discussed in the next section.

### 3 Numerical method

Our numerical approach is based on the streamfunction–vorticity method used by Blyth et al. [1] which took as its foundation the method proposed of E and Liu [14] for two-dimensional Navier–Stokes calculations. First, we introduce the new coordinate  $\eta = y/H_0(t)$  so that the vertical spatial domain now occupies the fixed interval  $-1 \leq \eta \leq 1$ . It is then convenient to introduce the new variables

$$T_0 = -\frac{1}{H_0^2} F_{0\eta\eta}, \quad T_1 = -\frac{1}{H_0^2} F_{1\eta\eta}, \quad (18)$$

in which case (6) becomes

$$T_{0t} - \frac{\dot{H}_0}{H_0} \eta T_{0\eta} + \frac{1}{H_0} (F_{0\eta} T_0 - F_0 T_{0\eta}) = \frac{1}{RH_0^2} T_{0\eta\eta}. \quad (19)$$

and (12) becomes

$$T_{1t} - \frac{\dot{H}_0}{H_0} \eta T_{1\eta} + \frac{1}{H_0} (F_{1\eta} T_0 - 2F_1 T_{0\eta}) + \frac{1}{H_0} (2F_{0\eta} T_1 - F_0 T_{1\eta}) = \frac{1}{RH_0^2} T_{1\eta\eta}. \quad (20)$$

The equations (19) and (20) are discretised using centred differences on the uniform grid  $\eta_i = -1 + (i-1)h$ ,  $i = 1, \dots, N$ , where  $h = 2/(N-1)$  for integer  $N$ . At the  $k$ th time step, the equations are integrated forward from  $t = t_k = k \, dt$  to  $t_{k+1}$  using a fourth-order Runge–Kutta method analogous to that presented in section 3 of Blyth et al. [1]. The tridiagonal discretised forms of (18) are then solved using the Thomas algorithm to obtain estimates for  $F_{0,i}^k$  and  $F_{1,i}^k$  at the  $i$ th grid point at time step  $k$ . During this procedure, we apply the boundary conditions (13) and also the end conditions

$$\begin{aligned} T_{0,1}^k &= -\frac{2}{h^2 H_0^2(t_k)} (F_{0,2}^k - \dot{H}_0(t_k)), \\ T_{0,N}^k &= -\frac{2}{h^2 H_0^2(t_k)} (F_{0,N-1}^k + \dot{H}_0(t_k)), \end{aligned} \quad (21)$$

and

$$\begin{aligned} T_{1,1}^k &= \frac{1}{H_0^2(t_k)} \left[ \frac{4H_1(t_k)}{h^3 H_0(t_k)} (F_{0,2}^k - \dot{H}_0(t_k)) - \frac{1}{h^2} (2F_{1,2}^k - \dot{H}_1(t_k)) \right], \\ T_{1,N}^k &= \frac{1}{H_0^2(t_k)} \left[ \frac{4H_1(t_k)}{h^3 H_0(t_k)} (F_{0,N-1}^k + \dot{H}_0(t_k)) - \frac{1}{h^2} (2F_{1,N-1}^k + \dot{H}_1(t_k)) \right], \end{aligned} \quad (22)$$

which have been derived by first introducing fictitious points outside of the grid as in Blyth et al. [1]. The numerical solution for the system (14), (15) over the fixed  $\eta$  grid is obtained in a similar way. For the calculations to be presented in the next section, unless otherwise stated we used the time step and grid size  $dt = 5 \times 10^{-5}$  and  $N = 401$ . These values are found to be sufficient to obtain accurate solutions. Evidence for this is presented in Fig. 2.

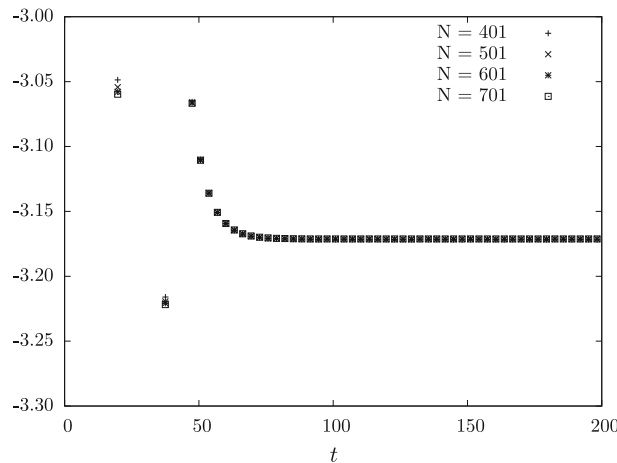


**Fig. 2** Plot of the minima of  $F_{1\eta\eta}(-1, t)/\exp(at)$  for various numbers of grid points,  $N$ , when  $\Delta = 0.65$ ,  $R = 40.0$ ,  $dt = 5 \times 10^{-5}$  and  $a = 0.166$

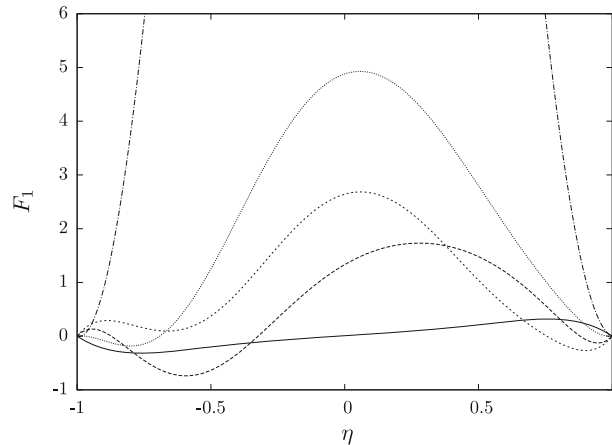


**Fig. 3** An illustration of the change in symmetry of  $F_1$  for the exponentially growing solutions. Here,  $\Delta = 0.5$ ,  $H_1 = 0.5$ ,  $R = 37$ , and we plot at times  $t = 30, 50, 60, 150$  and  $300$  (shown by increasing amplitude) starting from initial condition (B)

#### 4 Results

In the following discussion, we will refer to the channel flow with parallel walls ( $\delta = 0$ ) governed by (6), (7) as the HP flow, and we will refer to the solution of the problem governed by (12), (13) for slightly inclined walls as the tapering flow. For sufficiently small Reynolds number, the HP flow has a unique, stable,  $\pi$ -periodic solution which is synchronised with the wall motion and for which  $F_0$  is odd in  $\eta$ , so that the flow velocity is symmetric about  $\eta = 0$ . A symmetry-breaking bifurcation at Reynolds number  $R_0(\Delta)$  introduces a new, stable asymmetric solution, which is also synchronised with the wall motion and which coexists with the symmetric solution: for future reference, we label the symmetric solution  $F_0^S$ , which is odd in  $\eta$ , and the asymmetric solution  $F_0^A$ , which is even in  $\eta$ . As  $R$  increases, eventually a second critical value is reached at  $R = R_3(\Delta)$  at which a Hopf bifurcation occurs and new, asynchronous solutions emerge heralding a rich set of dynamics across the  $(\Delta, R)$  parameter space including quasiperiodic flow and chaotic flow reached via a Feigenbaum cascade.

To provide a focus for our study, we assume that the angle of tilt of the channel walls is fixed during the motion so that  $H_1$  is constant (as noted above, the particular value of the constant does not matter). We performed a large number of numerical simulations starting from initial conditions chosen from the set (A, B):

$$(A) \quad F_0 = F_1 = 0, \quad (B) \quad F_0 = F_1 = -(\eta + 1)^2(\eta - 1)^3, \quad (23)$$

where the latter condition (B) has been devised to be asymmetric across the channel.

Similar to HP's findings, for sufficiently small Reynolds number, a unique  $\pi$ -periodic solution for  $F_1$  exists, which is synchronised with the wall motion; furthermore,  $F_1$  is odd in  $\eta$  so that the flow velocity is symmetric about the channel centreline. At  $R = R_1(\Delta)$ , where  $R_1 < R_0$ , the solution is no longer synchronous with the wall, and instead, we find that  $F_1$  has the Floquet structure

$$F_1(\eta, t) = e^{at} \tilde{F}_1(\eta, t), \quad (24)$$

where  $\tilde{F}_1$  is  $\pi$ -periodic in  $t$  and  $a$  is a real, positive constant (note that at higher Reynolds number we may find complex values of  $a$ ). Consequently, the solution blows up exponentially as  $t \rightarrow \infty$ . Starting from initial condition (B), during the blow-up, the solution for  $F_1$  evolves as time progresses from its initially asymmetric state to being odd in  $\eta$  to being asymmetric again and ultimately to being even (see, for example, Fig. 3). So the solution loses its symmetry about the channel centreline simultaneously with the onset of exponential blow-up. Note that this occurs at Reynolds numbers below the symmetry-breaking bifurcation point  $R_0$  for the HP flow.

Assuming that it is real, the rate of exponential growth  $a$  can be estimated from a specific numerical simulation, once initial transients have decayed, by computing

$$a = \frac{1}{\pi} \log \left( \frac{F_{1\eta\eta}(-1, t + \pi)}{F_{1\eta\eta}(-1, t)} \right). \quad (25)$$

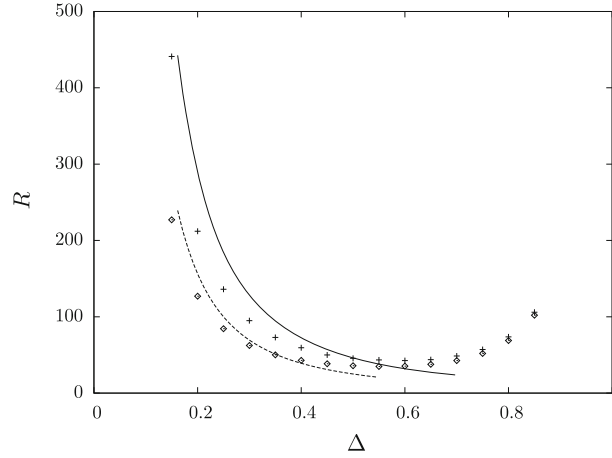


**Fig. 4** Critical values in  $(\Delta, R)$  space: the *diamonds* ( $\diamond$ ) indicate  $R_1$  at which  $a$  becomes positive and the exponential growth in  $F_1$  (and a simultaneous loss of symmetry) sets in. The *crosses* (+) indicate the symmetry-breaking bifurcation at  $R = R_0$  for the HP parallel-channel flow and are taken from the data in HP. The *solid* and *the broken lines* are the asymptotic predictions  $R_0 = (3.4/\Delta)^2$  and  $R_1 = (2.5/\Delta)^2$  from the steady-streaming analysis of HP and Sect. 5, respectively

By choosing a sufficiently large Reynolds number at which exponential growth occurs and then stepping backwards to find the Reynolds number where  $a = 0$ , we can estimate the location of  $R_1$ . In Fig. 4, we show results of our calculations to determine  $R_1$  over a range of values of wall amplitude  $\Delta$ . It appears from the results that  $R_1 < R_0$  so that the transition to exponentially blowing-up, asymmetric flow for the tapering flow always occurs at a lower Reynolds number than the symmetry breaking for the HP flow.

The dynamics for  $R > R_0$  depend on the choice made for  $F_0$ . Taking  $F_0 = F_0^S$ , solutions are found to grow exponentially in time with the basic structure (24) and with  $\tilde{F}_1$  asymmetric in  $\eta$ . Taking instead  $F_0 = F_0^A$ , we find for any  $\Delta$  a window  $R_0 \leq R \leq R_2(\Delta)$  of stable,  $\pi$ -periodic solutions which are synchronous with the wall and which are asymmetric about the channel centreline. The  $\pi$ -periodic solution destabilises at  $R = R_2$ , and beyond this, the  $F_1$  flow grows exponentially in time according to the structure (24) with  $\text{Re}(a) > 0$  and  $\text{Im}(a) \neq 0$ . Interestingly, the broad features of the flow (with the exponential growth in time factored out) for  $R > R_2$  follow those identified by HP for the parallel-wall case, so that  $\exp(-a_r t) F_1$  becomes quasiperiodic for smaller  $\Delta$ , and  $\exp(-a_r t) F_1$  undergoes period doubling for larger  $\Delta$ , where  $a_r = \text{Re}(a)$ , but the onset of quasiperiodic behaviour for the taper flow generally occurs at a smaller Reynolds number than for the HP flow, so that  $R_2 < R_3$ . This is illustrated, together with the other general features already discussed, in Figs. 7 and 8 for the cases  $\Delta = 0.25$  and  $\Delta = 0.65$ . The finer details of these two cases are discussed in the following paragraphs.

Figure 5a shows how the maxima of the time signal  $T_1(1, t)$  for the tapering flow increase exponentially for the case  $\Delta = 0.25$  and  $R = 100 < R_0$ . In the figure, the time signal  $L = \log(m)$  is plotted against time  $t$ , where  $m = \max |T_1(1, t)|$  are the local maxima in the time signal of  $T_1$  at the upper wall. The numerical data are separated by a distance  $\pi$  in  $t$ , indicating that the exponent  $a$  is real, and lie along a straight line of slope  $a = 0.0258$ , which is determined by making a best-fit straight line through the time signal data. Figure 5b shows the time signal  $L$  plotted against time for  $\Delta = 0.25$  and for the larger Reynolds number  $R = 200$ , which lies inside the stable  $\pi$ -periodic window  $[R_0, R_2] = [136, 254]$ . After an initial exponentially growing phase, the signal attenuates via an exponentially decaying, irregular transient to a  $\pi$ -periodic state, whose corresponding  $F_1$  profile (not shown) is asymmetric across the channel. The emergence of the  $\pi$ -periodic state can be seen more clearly in the lower of the two insets inside the figure.

The upper inset shows the return map of the exponentially decaying part of the  $L$  signal, obtained by plotting pairs  $(p_i, p_{i+1})$ , where the  $p_i$  is the local maxima of  $L - a_r t$ , where  $a_r$  is the real part of the exponent of the decaying phase, which is estimated from the data to be  $a_r = -0.032$ . The structure of the return map suggests that the decaying phase is quasiperiodic in character once the exponentially decaying part has been extracted. This is interesting as it is a first sign of quasiperiodic behaviour in the tapering flow (we note that there is no indication of similar behaviour in the corresponding HP flow, which approaches the periodic state at this Reynolds number via a regular transient; quasiperiodic transients occur for the HP flow at higher Reynolds number for this  $\Delta$ ). Continuing to higher Reynolds number, we find that at  $R = R_2 \approx 255$  the tapering flow

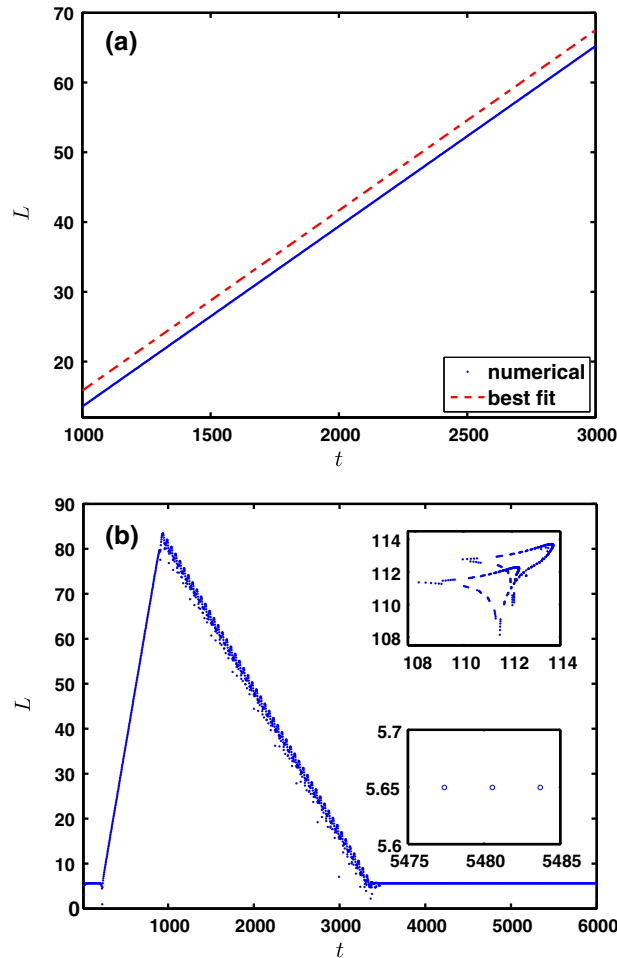


**Fig. 5**  $L = \log(m)$  versus  $t$ , where  $m = \max |T_1(1, t)|$  are the local maxima in the time signal of  $T_1$  at the upper wall for **a**  $\Delta = 0.25$  and  $R = 100$  and **b**  $\Delta = 0.25$  and  $R = 200$ . In **a**, the slope of the best-fit broken line is the Floquet exponent  $a = 0.0258$ . In **b**, the *lower inset* shows a close-up of the signal once the periodic state has been reached, and the *upper inset* is the return map of the exponentially decaying part of the signal between  $t = 933$  and  $t = 3,376$

function  $F_1$  once again grows exponentially in time but now  $\text{Re}(a) > 0$ ,  $\text{Im}(a) \neq 0$ . Evidence for this is presented in Fig. 6 which shows  $L$  versus  $t$  for  $\Delta = 0.25$  and  $R = 254$ . Evidently, there is no growth so that  $a_r = 0$ . Moreover, the inset in the figure shows that the return map  $(p_i, p_{i+1})$  exhibits a very similar structure to that seen in Fig. 5b and is strongly suggestive of quasiperiodic behaviour and an imaginary value of  $a$ .

For  $\Delta = 0.65$ , the HP parallel-wall flow loses symmetry at  $R_0$  and later encounters a Hopf bifurcation at  $R_3$ , beyond which the asymmetric solution  $F_0^A$  undergoes a period-doubling Feigenbaum cascade. The taper flow is  $\pi$ -periodic in the range  $44 < R < 49$ . At  $R = 49$ , exponential growth sets in; nonetheless, it is interesting to note that the reduced streamfunction  $\exp(-a_r t) F_1$  becomes  $2\pi$ -periodic so that an effective period doubling has taken place. As the Reynolds number is increased to  $R_3$  and beyond, the reduced streamfunction undergoes period doubling along with the HP flow as it passes through its Feigenbaum cascade. Beyond the Feigenbaum cascade, HP presented strong numerical evidence that  $F_0$  becomes chaotic. It seems clear that a chaotic  $F_0$  in (12), (13) will force a chaotic response in the taper flow; through careful calculations, we have confirmed that when  $F_0^A$  is chaotic,  $\exp(-a_r t) F_1$  is also chaotic as expected (see Rickett [10] for further details).

EP-computed solutions of the parasitic equation (8) and showed that for  $\Delta$  below a threshold value, bounded symmetric solutions first lose stability to asymmetric solutions before a bifurcation to exponentially growing solutions occurs at higher Reynolds number. This contrasts with the tapering flow for which the onset of asymmetry and exponential growth occurs at the same Reynolds number,  $R = R_1$ . EP delineated the curve in  $\Delta - R$  parameter space which separates bounded, wall-synchronous solutions from those with exponential growth. This curve exhibits a fold so that for a fixed value of  $\Delta$ , as  $R$  is increased, the solution changes from

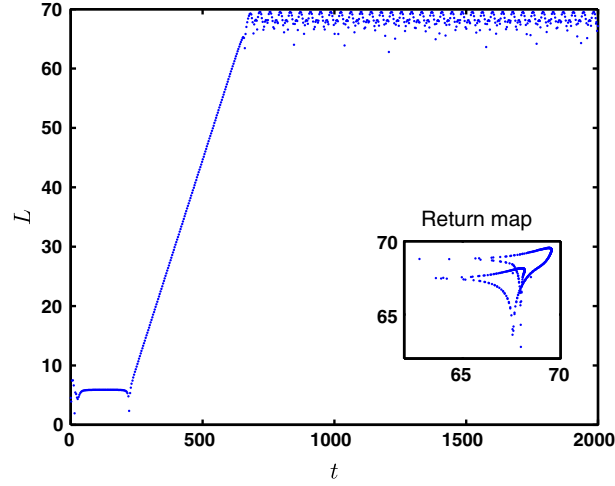


**Fig. 6**  $\Delta = 0.25$ ,  $R = 254$ , bounded quasiperiodic flow:  $L$  versus  $t$  (see caption to Fig. 5 for definition of  $L$ ). The inset shows the return map of the maxima  $m$

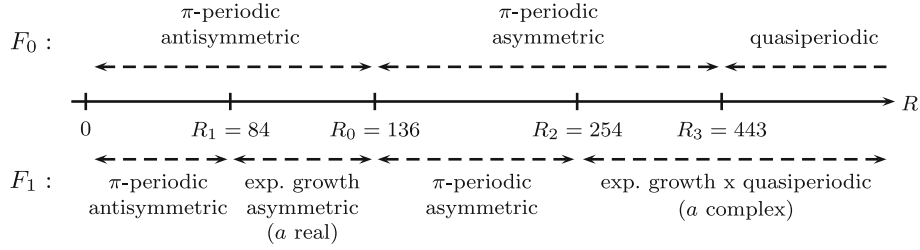


**Fig. 7** The generic behaviour of  $F_0$  and  $F_1$  for  $\Delta = 0.25$ . Note that the stated behaviour for  $F_1$  is on the assumption that  $F_0$  adopts its corresponding stable solution given directly above. From our calculations, the parallel-wall HP flow becomes quasiperiodic at  $R \approx 443$  compared with  $R \approx 544$  found by HP. The discrepancy in these values is discussed in detail in the ‘‘Appendix’’

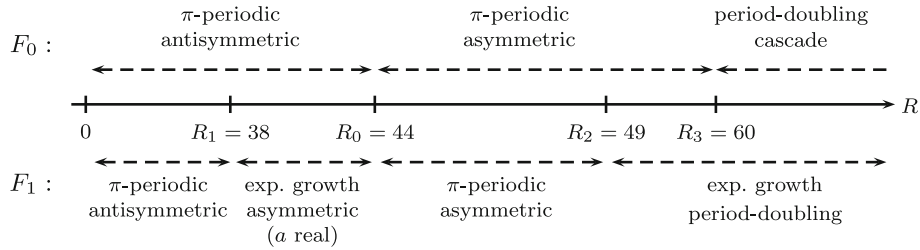


**Fig. 8** The generic behaviour of  $F_0$  and  $F_1$  for  $\Delta = 0.65$ . Note that the stated behaviour for  $F_1$  is on the assumption that  $F_0$  adopts its corresponding stable solution given directly above

synchronous symmetric to exponentially growing to synchronous asymmetric to exponentially growing again (see their Fig. 1). No such fold appears to be present in the current problem (see Fig. 4; the diamonds are equally spaced by 0.05 along the  $\Delta$  axis).

We now briefly discuss the dynamics for the secondary system (14), (15). Since the tapering flow function  $F_1$  appears explicitly in (14), we expect any exponential growth in  $F_1$  to force exponential growth in  $G_1$  (with a structure analogous to (24) with  $F$  replaced by  $G$ ), and this is what we find. In fact, we found that loss of symmetry always occurs at the same Reynolds number as for  $F_1$  but that exponential growth in  $G_1$  occurs at a Reynolds number less than or equal to that for  $F_1$ . For example, when  $\Delta = 0.65$ , for which  $R_1 = 38$ , we find that  $G_1$  blows up when  $R > 7.6$ . In the range  $7.6 < R < 38$ , the exponentially growing solution for  $G_1$  is symmetric, but for  $R > 38$  the solution for  $G_1$  evolves over time from being symmetric to being asymmetric. We have seen that a window of  $\pi$ -periodic solutions exists for  $F_1$  inside the range  $R_1 < R < R_2$  (see Figs. 7, 8). In some cases, bounded solutions also exist for the  $G_1$  flow, but inside a narrower sub-window  $[R_1, R^*]$  with  $R^* < R_2$ . For example, taking the  $\pi$ -periodic, asymmetric solution for  $F_1$  in the window for

$\Delta = 0.25$ , we find that  $R^* = 161$  so that the solution for  $G_1$  is periodic for  $136 < R < 161$ , but exponential growth occurs for  $R > 161$ , with  $a$  real and  $\tilde{G}$  is  $\pi$ -periodic function of time. However, in other cases, no bounded solutions exist for  $G_1$  inside the corresponding window of  $\pi$ -periodic  $F_1$  solutions. For example, when  $\Delta = 0.65$ , there are no bounded solutions for  $G_1$  when  $R > 7.6$ .

### 5 The limit $\Delta \rightarrow 0$ , $R^{1/2}\Delta = O(1)$

HP examined the parallel-channel flow in the asymptotic limit  $\Delta \rightarrow 0$  and  $R^{1/2}\Delta = O(1)$  and demonstrated that Stokes layers at either wall drive a steady-streaming motion in a layer occupying the main part of the channel. Working in the same asymptotic limit, we write

$$\Delta = dR^{-1/2}, \quad (26)$$

for some  $O(1)$  constant  $d$ . Our goal here is to establish asymptotic results to support some of the observations made for  $O(1)$  values of  $\Delta$  in Sect. 4.

It is convenient to rewrite the governing equations by introducing the coordinate  $\eta = y/H_0(t)$  and making the transformations  $F_0 = -\dot{H}_0\eta + H_0^3 f(\eta, t)$ , as in HP, and  $F_1 = H_0^4 H_1 g(\eta, t)$  for new functions  $f$  and  $g$ , and for constant  $H_1$ . Then, the system (6), (7) becomes equivalently

$$f_{\eta\eta t} + H_0^2 (f_\eta f_{\eta\eta} - f f_{\eta\eta\eta}) = \frac{1}{RH_0^2} f_{\eta\eta\eta\eta}, \quad (27)$$

with

$$f(\pm 1, t) = 0, \quad f_\eta(\pm 1, t) = \frac{\dot{H}_0}{H_0^3}, \quad (28)$$

and the system (12), (13) becomes equivalently

$$g_{\eta\eta t} - H_0^2 (2f_{\eta\eta\eta}g - f_{\eta\eta}g_\eta - 2f_\eta g_{\eta\eta} + f g_{\eta\eta\eta}) = \frac{1}{RH_0^2} g_{\eta\eta\eta\eta}, \quad (29)$$

with

$$g(\pm 1, t) = 0, \quad g_\eta(\pm 1, t) = \mp \frac{1}{H_0^3} f_{\eta\eta}(\pm 1, t). \quad (30)$$

Note that the constant  $H_1$  has been scaled from the problem.

For  $R$  large we anticipate the presence of Stokes layers at the walls. Concentrating on the upper wall, we introduce the Stokes layer variable  $\zeta = R^{1/2}(1 - \eta)$ , where  $\zeta = O(1)$  and expand by writing

$$f = R^{-1} \tilde{f}_0(\zeta, t) + R^{-3/2} [\tilde{f}_1(\zeta, t) + \tilde{f}_{1M}(\zeta)] + R^{-2} [\tilde{f}_2(\zeta, t) + \tilde{f}_{2M}(\zeta)] + \dots, \quad (31)$$

$$g = R^{-1/2} \tilde{g}_0(\zeta, t) + R^{-1} [\tilde{g}_1(\zeta, t) + \tilde{g}_{1M}(\zeta)] + R^{-3/2} [\tilde{g}_2(\zeta, t) + \tilde{g}_{2M}(\zeta)] + \dots, \quad (32)$$

where  $f_1, g_1, f_2$  and  $g_2$  are assumed to be time periodic with zero average over one time period. The form of these expansions is informed by the assumed scalings on  $R$  and  $\Delta$  and by the boundary conditions (28) and (30). At leading order, we find

$$\tilde{f}_0 = \frac{di}{(1+i)} e^{2it} (e^{-(1+i)\zeta} - 1) + \text{c.c.}, \quad \tilde{g}_0 = -di e^{2it} (e^{-(1+i)\zeta} - 1) + \text{c.c.}, \quad (33)$$

where c.c. denotes the complex conjugate. At first order, we obtain

$$\tilde{f}_{1M} = d^2 \left[ \frac{(1+i)}{2} (e^{-(1+i)\zeta} - 1) + \frac{(1+i)}{4} (e^{-(1-i)\zeta} - 1) + \text{c.c.} + \frac{1}{4} (e^{-2\zeta} - 1) + \frac{3}{2}\zeta \right], \quad (34)$$

$$\tilde{g}_{1M} = -d^2 \left[ \frac{1}{2} (e^{-(1+i)\zeta} - 1) + \text{c.c.} + \frac{1}{2} (e^{-2\zeta} - 1) - \frac{1}{2} \right], \quad (35)$$

and

$$\begin{aligned} \tilde{f}_1 = & \frac{3(1+i)d^2}{4} \left[ \sqrt{2} \left( e^{-\sqrt{2}(1+i)\zeta} - 1 \right) - \left( e^{-(1+i)\zeta} - 1 \right) \right] e^{4it} \\ & + \frac{di}{(1+i)} \left[ \frac{1}{\sqrt{2}(1+i)} \left( e^{-\sqrt{2}(1+i)\zeta} - 1 \right) + \zeta \right] e^{2it} + \text{c.c.}, \end{aligned} \quad (36)$$

$$\begin{aligned} \tilde{g}_1 = & -\frac{id^2}{2} \left[ 6 \left( e^{-\sqrt{2}(1+i)\zeta} - 1 \right) - 5 \left( e^{-(1+i)\zeta} - 1 \right) \right] e^{4it} \\ & - \left[ \frac{di}{(1+i)} \left( e^{-\sqrt{2}(1+i)\zeta} - 1 \right) - di \left( \frac{1}{\sqrt{2}(1+i)} \left( e^{-\sqrt{2}(1+i)\zeta} - 1 \right) + \zeta \right) \right] e^{2it} + \text{c.c.} \end{aligned} \quad (37)$$

The solutions  $\tilde{f}_0$ ,  $\tilde{f}_1$  and  $\tilde{f}_{1M}$  coincide with those found by HP.

As is usual in this type of analysis (see Stuart [13] and Riley [11]), a slip velocity persists at the edge of the Stokes layer which drives a mean streaming motion beyond. In the present case, this slip velocity is apparent from the observation that  $\lim_{\zeta \rightarrow \infty} f_{1M} = 3/2$ . Therefore, a steady-streaming layer is anticipated, and in the present case, it occupies the main part of the channel, that is where  $\eta = O(1)$  (see HP). Consistent with the expansions in the Stokes layer, the flow variables in the steady-streaming layer expand as

$$f = R^{-1} \left[ f_0(\eta, t) + \phi(\eta, \tau) \right] + R^{-3/2} f_1(\eta, t) + R^{-2} f_2(\eta, t) + \dots, \quad (38)$$

$$g = R^{-1/2} g_0(\eta, t) + R^{-1} \left[ g_1(\eta, t) + \psi(\eta, \tau) \right] + R^{-3/2} g_2(\eta, t) + R^{-2} g_3(\eta, t) + \dots, \quad (39)$$

where  $f_0$ ,  $g_0$  and  $f_1$ ,  $g_1$  are time periodic with zero mean. Notice that the second terms in the square brackets depend on the new, slow modulational time variable  $\tau = t/R$ .

At leading order and first order, we find

$$f_0 = A_0(t)\eta + B_0(t), \quad g_0 = C_0(t)\eta + D_0(t), \quad (40)$$

$$f_1 = A_1(t)\eta + B_1(t) + C_1(\eta), \quad g_1 = D_1(t)\eta + E_1(t) + F_1(\eta). \quad (41)$$

We substitute these forms and the expansions (38), (39) into the governing equations (27) and (29) and take the time average over one  $t$  time period. Making the transformations  $\phi \rightarrow (3d^2/2)\phi$ ,  $\psi \rightarrow (3d^2/2)\psi$  and  $\tau \rightarrow (3d^2/2)^{-1}\tau$ , we derive the steady-streaming problems

$$\phi_{\eta\eta\tau} + \phi_\eta \phi_{\eta\eta} - \phi \phi_{\eta\eta\eta} = \frac{1}{R_s} \phi_{\eta\eta\eta\eta}, \quad \phi(\eta = \pm 1) = 0, \quad \phi_\eta(\eta = \pm 1) = -1, \quad (42)$$

and

$$\begin{aligned} \psi_{\eta\eta\tau} - 2\phi_{\eta\eta}\psi + \phi_{\eta\eta}\psi_\eta + 2\phi_\eta\psi_{\eta\eta} - \psi\psi_{\eta\eta\eta} &= \frac{1}{R_s} \psi_{\eta\eta\eta\eta}, \\ \psi(\eta = \pm 1) &= \pm \frac{4}{3}, \quad \psi_\eta(\eta = \pm 1) = \mp \phi_{\eta\eta}(\eta = \pm 1) + \frac{13}{9} 2^{1/2}, \end{aligned} \quad (43)$$

where  $R_s = 3d^2/2$  is the steady-streaming Reynolds number. For the HP steady-streaming problem, the second of the boundary conditions in (42) implies that the steady horizontal slip velocity generated by the Stokes layer is directed towards the origin. Both of the systems (42) and (43) support an antisymmetric steady solution which is expected to be unique when  $R_s$  lies below a threshold value. Expanding for small  $R_s$ , we obtain the steady forms

$$\phi = \frac{1}{2} (\eta - \eta^3) + O(R_s), \quad \psi = \left( \frac{1}{2} - \frac{13}{18} \sqrt{2} \right) \eta + \left( \frac{5}{6} + \frac{13}{18} \sqrt{2} \right) \eta^3 + O(R_s). \quad (44)$$

In general, we label the steady solutions to (42) and (43)  $\phi_B$  and  $\psi_B$ , respectively.

To examine the linear stability of the steady solutions, we write

$$\phi = \phi_B(\eta) + \hat{\phi}(\eta, \tau), \quad \psi = \psi_B(\eta) + \hat{\psi}(\eta, \tau), \quad (45)$$

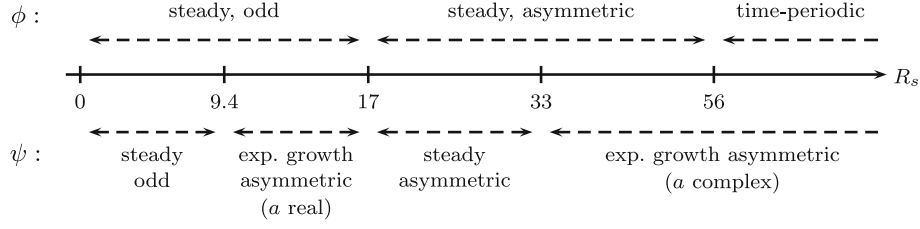


**Fig. 9** The generic behaviour of  $\phi$  and  $\psi$  for different ranges of  $d$ . Note that the stated behaviour for  $\psi$  is on the assumption that  $\phi$  adopts its corresponding stable solution given directly above

where  $\hat{\phi}$  and  $\hat{\psi}$  are small in magnitude and satisfy the linearised systems

$$\begin{aligned} \hat{\phi}_{\eta\eta\tau} + \phi_{B\eta}\hat{\phi}_{\eta\eta} + \phi_{B\eta\eta}\hat{\phi}_{\eta} - \phi_B\hat{\phi}_{\eta\eta\eta} - \phi_{B\eta\eta\eta}\hat{\phi} &= \frac{1}{R_s}\hat{\phi}_{\eta\eta\eta\eta}, \\ \hat{\phi}(\eta = \pm 1) &= 0, \quad \hat{\phi}_{\eta}(\eta = \pm 1) = 0, \end{aligned} \quad (46)$$

and

$$\begin{aligned} \hat{\psi}_{\eta\eta\tau} - 2\left(\phi_{B\eta\eta\eta}\hat{\psi} + \psi_B\hat{\phi}_{\eta\eta\eta}\right) + \phi_{B\eta\eta}\hat{\psi}_{\eta} + \psi_{B\eta}\hat{\phi}_{\eta\eta} + 2\left(\phi_{B\eta}\hat{\psi}_{\eta\eta} + \psi_{B\eta\eta}\hat{\phi}_{\eta}\right) \\ - \left(\phi_B\hat{\psi}_{\eta\eta\eta} + \psi_{B\eta\eta\eta}\hat{\phi}\right) &= \frac{1}{R_s}\hat{\psi}_{\eta\eta\eta\eta}, \\ \hat{\psi}(\eta = \pm 1) &= 0, \quad \hat{\psi}_{\eta}(\eta = \pm 1) = \mp\hat{\phi}_{\eta\eta}(\eta = \pm 1). \end{aligned} \quad (47)$$

These are solved numerically by marching forwards in time using a procedure similar to that described earlier and using a symmetric initial condition for both  $\hat{\phi}$  and  $\hat{\psi}$ .

When  $R_s = 17$  ( $d = 3.4$ ), the HP linearised system (46) predicts the appearance of a stable, steady, symmetric mode  $\hat{\phi}$  so that, overall, the solution for  $\phi$  becomes asymmetric. We note that our results predict the critical value to be  $d = 3.4$  in agreement with Watson et al. [17]. The linearised system (47) for the taper flow also predicts that the antisymmetry of the basic flow  $\psi_B$  is broken and that it occurs at the lower value of  $R_s = 9.4$  ( $d = 2.5$ ) at which point a stable, symmetric mode  $\hat{\psi}$  appears.

Solving instead the full systems (42) and (43) numerically, we confirm that a symmetry-breaking bifurcation occurs for the nonlinear system (42) at  $R_s = 17$  ( $d = 3.4$ ) giving rise to a steady solution for  $\phi$  which is asymmetric across the channel (as found by HP), and the solution to (43) loses symmetry at  $R_s = 9.4$  ( $d = 2.5$ ) and the solution for  $\psi$  grows exponentially in time. Starting from an initial condition for  $\psi$  which is odd in  $\eta$ , we see that as time progresses the solution changes to being antisymmetric to being asymmetric and then to being symmetric as the exponential growth takes hold, and this is in line with the predictions of the linearised analysis presented in the previous paragraph. Moreover, it offers an interpretation of the qualitatively similar behaviour which was observed in simulations of the full system in Fig. 3. Furthermore, the present results reinforce the observation made in Sect. 4 that the tapering flow loses symmetry before the parallel-wall HP flow. The present asymptotic predictions for the loss of symmetry are compared with the results of the earlier numerical simulations in Fig. 4.

When  $R_s > 17$  and  $\phi$  is asymmetric, we find that it is possible to obtain a steady, asymmetric solution for  $\psi$ . This is similar to the results for the full problem in Sect. 4, where it was found to be possible to obtain a bounded solution for the tapering flow above the symmetry-breaking bifurcation for the HP flow. At  $R_s = 56$  ( $d = 6.1$ <sup>1</sup>), the HP system (46), with  $\phi_B$  taken to be the asymmetric solution, undergoes a Hopf bifurcation and a time-periodic solution emerges. As was noted by HP, since the newly introduced frequency corresponds to a long time period on an  $O(R)$  scale, the overall flow is quasiperiodic. Time-periodic behaviour also emerges for the tapering system (47), but at around the lower value  $R_s = 33$  ( $d = 4.7$ ).

Returning to the full equations (42) and (43), we obtain confirmation of these findings. The behaviour is summarised in Fig. 9. When  $9.4 < R_s < 17$ ,  $\psi$  experiences exponential growth in time and, in particular, adopts the Floquet form

<sup>1</sup> We note that HP computed  $d = 5.99$  at this boundary; our computation of  $d = 6.1$  is in agreement with that of Watson et al. [17].

$$\psi(\eta, t) = e^{at} \tilde{\psi}(\eta), \quad (48)$$

where  $a$  is a real number. Inside the window  $17 < R_s < 33$  a steady, asymmetric solution for  $\psi$  is found if  $\phi$  adopts the stable, asymmetric solution which appears beyond the symmetry-breaking bifurcation at  $d = 3.4$  (note that if instead, and through a careful choice of initial conditions,  $\phi$  is taken to be the coexisting odd solution, then  $\psi$  grows exponentially in time inside this window).

For  $R_s > 33$ ,  $\psi$  grows exponentially in time with the structure (48) but now  $a$  is complex so that the growth is oscillatory in nature; the HP  $\phi$  flow becomes periodic at  $R_s = 56$ . Since the present analysis is performed on a long  $O(R)$  timescale, the overall HP flow is quasiperiodic and the overall tapering flow is exponentially growing modulated by a quasiperiodic function. So the onset of quasiperiodicity occurs earlier in  $R_s$  for the tapering flow than for the HP flow. These findings are in line with the discussion of the full system in Sect. 4. For  $R_s > 56$ , HP carefully charted a period-doubling cascade to chaos for  $\phi$ . We have not identified any cases for  $R_s > 56$  for which  $\psi$  does not grow exponentially in time.

## 6 Discussion

We have considered flow in a channel whose walls are inclined at a slight angle to each other and which are oscillating perpendicular to the channel centreline. For zero wall inclination angle, we recover the exact similarity solution of the Navier–Stokes equations discussed in detail by Hall and Papageorgiou [6] (HP). For the HP channel problem, the similarity solution space has a rich structure where periodic, synchronous (with the wall motion) flow gives way to asymmetric, aperiodic flow and ultimately chaotic flow as the Reynolds number is increased. The flow adjustment due to the wall taper is governed by a linearised set of partial differential equations with coefficients which depend on the base HP solution and, consequently, non-trivial dynamics are anticipated. Certainly, it is expected that when the HP flow becomes asymmetric, the taper flow adjustment would follow suit. In fact, what we have found that symmetry loss for the tapering flow may occur at a lower Reynolds number than for the parallel-wall flow.

For sufficiently small Reynolds number, the flow in the tapering channel is unique, is periodic with the same period as the wall motion and is symmetric about the channel centreline. At the same critical Reynolds number at which the centreline symmetry is lost, the taper flow adjustment becomes unbounded and grows exponentially in time, signalling the breakdown of our assumed flow structure. At higher Reynolds number, there is a second window of periodic taper flow solutions; these are asymmetric with respect to the channel centreline and synchronous with the oscillating walls. The periodic state is reached after a long transient, indicating a complex Floquet exponent with negative real part. At the upper end of the window, the flow destabilises as the complex Floquet exponent passes into the right-half complex plane. For smaller values of  $\Delta$ , the reduced flow is quasiperiodic at the upper bound of the window, indicating an imaginary Floquet exponent incommensurate with the wall driving frequency; for larger  $\Delta$ , a period doubling occurs at the upper boundary of the window. These generic features qualitatively reflect those found for the parallel-wall flow, but it is worth emphasising that the changes in behaviour (e.g. from symmetric to asymmetric flow) tend to occur at lower Reynolds number for the taper flow so that inclining the channel walls tends to push the stability boundaries to lower  $R$ .

In related work, Espin and Papageorgiou [2] (EP) studied the  $x$ -independent parasitic flow which is driven by an arbitrary pressure gradient and which can be superposed onto the parallel-wall flow. This  $x$ -independent flow is affected by the HP flow solution (via the coefficients in the linear partial differential equations which govern it) but not vice versa. For a constant pressure gradient, EP's findings have some striking similarities to those obtained here for the tapering flow. Notably, as the Reynolds number is increased, the parasitic flow loses symmetry before the HP flow does. Exponential growth in time (due, as here, to a positive Floquet exponent) occurs over much of  $(\Delta, R)$  parameter space, and asymmetric solutions, which are synchronous with the wall motion, are also possible. Notably, in our problem, the transition from synchronous, symmetric flow to asymmetric flow with exponential growth occurs simultaneously, and this is not so in the EP problem. Also, EP identified a fold in the curve dividing bounded solutions from those experiencing exponential growth, and no such fold has been found here.

According to the expansion (10), our analysis holds for order one values of  $x$ , but breaks down on the long axial length scale  $x = O(1/\delta)$ , where  $\delta$  is the small angle of inclination of the channel walls. In a long but finite tapering channel, and with some appropriate boundary conditions imposed at the channel ends, it might be anticipated that the stable flows which we have computed could be observed over some portion of the channel length. A recent investigation by Espin and Papageorgiou [3] lends some credibility to this idea. These

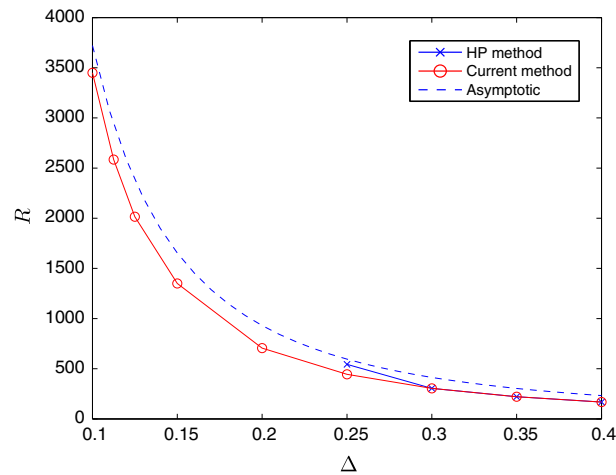


**Fig. 10** The location of the bifurcation to quasiperiodic HP flow (*circles* results from HP; *squares* present results; *broken line* the asymptotic result  $R = (6.1/\Delta)^2$  from Sect. 5)

authors conducted a numerical study of flow in a channel with accelerating or decelerating walls, for which there is known to be an exact similarity solution of the Navier–Stokes equations in the infinite channel case. The calculations they performed in a finite channel of large aspect ratio showed that the similarity solution is observed over at least part of length of the channel, depending on the boundary conditions at the channel ends, and provided the Reynolds number is sufficiently small. The relevance between this and the present problem is revealed in the small amplitude, high Reynolds number limit where, as was noted by HP and seen here through (42), the decelerating wall problem controls the flow in the steady-streaming layer for the oscillating wall problem. Espin and Papageorgiou’s [3] results are encouraging and suggest that our similarity-type tapering flow might indeed be observed in finite channel computations. It is also important to note, however, that recent studies by Hewitt and Hazel [7] and by Hewitt and Harrison [8] for axisymmetric flows have cast doubt over the relevance of some similarity forms to flow in finite domains.

## Appendix

We noted in Sect. 4 that our prediction for the transition from periodic to quasiperiodic flow for the parallel-walled channel flow differs from that quoted by HP. To investigate the discrepancy, we checked our calculations in a number of ways. Starting from a clean slate, we wrote independently two codes implementing the streamfunction–vorticity method presented in Sect. 3 and confirmed agreement with our initial results. We also wrote a code implementing the Crank–Nicolson type numerical method described in Sect. 3 of HP. We focused our investigations on the border between periodic and quasiperiodic flow over a range of values of the wall amplitude  $\Delta$ . The results are summarised in Fig. 10. Evidently, a larger number of grid points are needed for higher Reynolds number as thin boundary layers develop at the walls. Our computations were checked using up to  $N = 600$  grid points and using a smallest time step of size  $dt = 0.0001$ .

The blue crosses, representing the values given in HP, were confirmed by running our code based on the HP numerical method. It is striking that the present streamfunction–vorticity approach agrees with the HP method for the larger values of  $\Delta$  but, as has already been remarked, the two disagree markedly at  $\Delta = 0.25$ . For smaller values than this, we found that the Crank–Nicolson method becomes unreliable and the computed bifurcation points do not approach the asymptotic result from HP’s steady-streaming analysis (the broken line in the figure). In contrast, the results from the streamfunction–vorticity code follow nicely the asymptotic prediction (we computed down to  $\Delta = 0.1$ ). Having said this, we still obtain consistent results between the two different numerical approaches when computing the location of the symmetry-breaking bifurcation; the results using the present method are in line with those presented in HP (shown in Fig. 4). In conclusion, we believe that we have obtained strong evidence that the present numerical method performs well at larger Reynolds number and is successful in accurately computing the bifurcation from periodic to quasiperiodic flow down to small values of  $\Delta$ .

**References**

1. Blyth, M.G., Hall, P., Papageorgiou, D.T.: Chaotic flows in pulsating cylindrical tubes: a class of exact Navier–Stokes solutions. *J. Fluid Mech.* **481**, 187–213 (2003)
2. Espin, L., Papageorgiou, D.T.: Viscous pressure-driven flows and their stability in channels with vertically oscillating walls. *Phys. Fluids* **24**, 023604 (2012)
3. Espin, L., Papageorgiou, D.T.: Flow in a channel with accelerating or decelerating wall velocity: a comparison between self-similar solutions and Navier–Stokes computations in finite domains. *Phys. Fluids* **21**, 113601 (2009)
4. Grotberg, J.B.: Volume-cycled oscillatory flow in a tapered channel. *J. Fluid Mech.* **141**, 249–264 (2006)
5. Hall, P.: Unsteady viscous flow in a pipe of slowly varying cross-section. *J. Fluid Mech.* **64**, 209–226 (1974)
6. Hall, P., Papageorgiou, D.T.: The onset of chaos in a class of Navier–Stokes solutions. *J. Fluid Mech.* **393**, 59–87 (1999)
7. Hewitt, R.E., Hazel, A.L.: Midplane-symmetry breaking in the flow between two counter-rotating disks. *J. Eng. Math.* **57**, 273–288 (2007)
8. Hewitt, R.E., Harrison, I.: Exponential sensitivity to symmetry imperfections in an exact Navier–Stokes solution. *J. Eng. Math.* **57**, 273–288 (2007)
9. Marciani, L., Gowland, P.A., Spiller, R.C., Manoj, P., Moore, R., Young, P., Fillery-Travis, A.: Effect of meal viscosity and nutrients on satiety, intragastric dilution and emptying assessed by MRI. *Am. J. Physiol. Gastrointest. Liver Physiol.* **280**(6), G1227–G1233 (2001)
10. Rickett, L.M.: A Mathematical Analysis of Digestive Processes in a Model Stomach. Ph.D. Thesis, University of East Anglia (2013)
11. Riley, N.: Oscillating viscous flows. *Mathematika* **12**, 161–175 (1965)
12. Secomb, T.W.: Flow in a channel with pulsating walls. *J. Fluid Mech.* **88**, 273 (1978)
13. Stuart, J.T.: Double boundary layers in oscillatory viscous flows. *J. Fluid Mech.* **24**, 673–687 (1966)
14. Weinan, E., Liu, J.-G.: Vorticity boundary condition and related issues for finite difference schemes. *J. Comput. Phys.* **124**, 368–382 (1996)
15. Waters, S.L.: Solute uptake through the walls of a pulsating channel. *J. Fluid Mech.* **433**, 193–208 (2001)
16. Waters, S.L.: A mathematical model for the laser treatment of heart disease. *J. Biomed. Eng.* **37**, 281–288 (2004)
17. Watson, E.B.B., Banks, W.H.H., Zaturka, M.B., Drazin, P.G.: On transition to chaos in two-dimensional channel flow symmetrically driven by accelerating walls. *J. Fluid Mech.* **212**, 451–485 (1990)